Analog Space–Time Coding for Multiantenna Ultra-Wideband Transmissions

Liuqing Yang, *Student Member, IEEE,* and Georgios B. Giannakis, *Fellow, IEEE*

***Abstract*—Ultra-wideband (UWB) transmissions have well-documented advantages for low-power, peer-to-peer, and multiple-access communications. Space–time coding (STC), on the other hand, has gained popularity as an effective means of boosting rates and performance. Existing UWB transmitters rely on a single antenna, while ST coders have mostly focused on digital linearly modulated transmissions. In this paper, we develop ST codes for analog (and possibly nonlinearly) modulated multiantenna UWB systems. We show that the resulting analog system is able to collect not only the spatial diversity, but also the multipath diversity inherited by the dense multipath channel, with either coherent or noncoherent reception. Simulations confirm a considerable increase in both bit-error rate performance and immunity against timing jitter, when wedding STC with UWB transmissions.**

***Index Terms*—Diversity, multipath, noncoherent detection, pulse-position modulation (PPM), Rake, space–time coding (STC), timing jitter, ultra-wideband (UWB).**

I. Introduction

ULTRA-WIDEBAND (UWB) communications have attractive features for baseband multiple access, tactical wireless communications, and multimedia services [7], [14]. A UWB transmission consists of a train of very short pulses, where the information is encoded in the amplitude via pulse-amplitude modulation (PAM), or in the shift via pulse-position modulation (PPM); see, e.g., [8], [14], [19], [23]. Random time-hopping (TH) codes allow multiple users to access a UWB channel [14], [20]. The ultrashort pulse shaper, together with the data modulation, result in a transmitted signal with low-power spectral density spread across the ultrawide bandwidth.

Conveying information with ultrashort pulses, UWB transmissions can resolve many paths, and are thus rich in multipath diversity. This has motivated research toward designing Rake receivers to collect the available diversity, and thus enhance the performance of UWB communication systems [4], [21]. Since the received waveform contains many delayed and scaled replicas of the transmitted pulses, a large number of fingers is needed. Moreover, each of the resolvable waveforms undergoes a different channel, which yields a different gain on each multipath return [18]. As a result, the design and implementation of Rake reception entail estimation of a large number of channel parameters, and are thus complicated. On the other hand, multiantenna-based space–time (ST) coding is an effective technique to enable spatial diversity, and thus increase channel performance and/or capacity [1], [16], [17]. Existing UWB transmitters rely on a single antenna, while ST coders have so far focused primarily on digital transmissions.

Furthermore, UWB transmissions have been shown to be very sensitive to timing jitter in nonfading channels [10]. We have verified by simulations that even in multipath fading channels, UWB transmissions with Rake reception are particularly sensitive to mistiming. We will see, though, that employing multiple transmit and/or receive antennas is beneficial in enhancing the immunity against timing jitter.

In this paper, we develop an analog STC scheme for the *analog* multiantenna UWB systems, which is inspired by Alamouti's *digital* ST code that has been considered in narrowband wireless system standards [1]. For simplicity, a peer-to-peer scenario is addressed, so the random TH codes are omitted. Detailed analysis is carried out for the two-transmit one-receive antennas setup with PAM. The STC designs are then extended to the nonlinear PPM, and generalized in various directions. Different from [1], our analog STC schemes are tailored for dense multipath channels. With channel estimates available, either PAM or PPM multiantenna transmissions can be combined coherently with the Rake receiver and maximum-ratio combining (MRC) to collect both spatial diversity and multipath diversity. Noncoherent reception is also possible to collect joint diversity gains, while bypassing channel estimation. The resulting multiantenna system can be implemented with conventional analog UWB Rake receivers. Simulations testing various scenarios confirm a considerable increase in both bit-error rate (BER) performance and immunity to timing jitter, when wedding STC with UWB.

Reminiscent of existing ST codes for digital linear modulations [1], [16], our UWB-specific schemes are novel in three directions.

1) *Digital symbol-by-symbol versus analog within each symbol waveform*. Existing STC schemes operate on digital symbols, whereas our UWB-tailored STC approaches encode pulses within symbol waveforms; it is this UWB-specific aspect of our codes that enables enhanced space-multipath diversity gains.

Paper approved by Z. Kostic, the Editor for Wireless Communication of the IEEE Communications Society. Manuscript received August 7, 2002; revised July 24, 2003. This work was supported in part through collaborative participation in the Communications and Networks Consortium sponsored by the U. S. Army Research Laboratory under the Collaborative Technology Alliance Program, Cooperative Agreement DAAD19-01-2-0011. The U. S. Government is authorized to reproduce and distribute reprints for Government purposes notwithstanding any copyright notation thereon. This work was also supported in part by the National Science Foundation under Grant EIA-0324864. This paper was presented in part at the IEEE Conference on Ultra-Wideband Systems and Technologies, Baltimore, MD, May 2002.

The authors are with the Department of Electrical and Computer Engineering, University of Minnesota, Minneapolis, MN 55455 USA (e-mail: lqyang@ece.umn.edu; georgios@ece.umn.edu).

Digital Object Identifier 10.1109/TCOMM.2004.823644

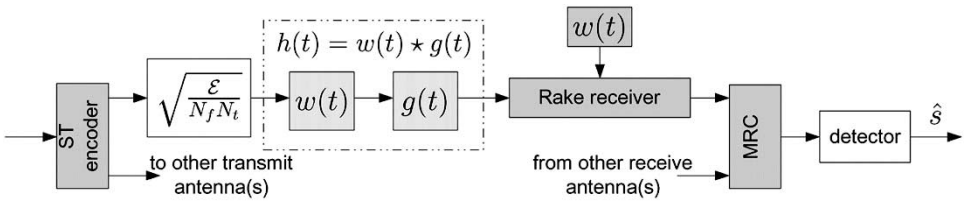

Fig. 1. Multiantenna UWB communication system model. Only one transmit antenna and one receive antenna are shown here.

2) *Flat or intersymbol interference (ISI)-inducing channels versus frequency-selective channels*. Existing STC schemes are designed either for flat or for ISI-inducing multiple-input/multiple-output (MIMO) fading channels, whereas our ST codes are tailored for non-ISI inducing UWB MIMO channels that are rich in multipath diversity.
3) *Linear and nonorthogonal nonlinear modulations versus linear and orthogonal nonlinear modulations with coherent or noncoherent reception*. Existing STC schemes entail linear modulators and coherent demodulators, except for [6], that deal with the noncoherent case. However, the latter do not consider orthogonal nonlinear modulations, which are of interest to UWB and lead to STC schemes that guarantee full diversity and symbol detectability, even with noncoherent reception.

The rest of the paper is organized as follows. In Section II, we introduce the channel model, the receiver structure, and the detection method through the analysis of a single-antenna UWB transmission. The performance criteria for our STC design are also presented in this section. Two analog STC schemes tailored for the two-transmit one-receive antennas setup are derived in Section III. In Section IV, we provide generalizations of our STC schemes in various aspects. Simulations are performed in Section V to verify our analyses and compare BER performance of our ST coded system with the conventional UWB system that deploys a single transmit antenna. Conclusions are drawn in Section VI.

II. System Model

In this section, we will introduce the UWB communication setup under consideration. The system model, including the modulation, channel model, receiver structure, and detection method, will be outlined through the analysis of a single-antenna transmission. We will also provide the performance criteria, namely, coding gain and diversity order. The performance of single-antenna transmissions not only serves as the motivation for our study of STC for UWB multiantenna communications, but also provides us with a benchmark for subsequent performance comparisons.

Consider the peer-to-peer UWB communication system shown in Fig. 1, where binary information symbols are conveyed by a stream of ultrashort pulses. With N_t denoting the number of transmit antennas, every binary symbol $s = \pm 1$ is power loaded, pulse shaped, and transmitted repeatedly over N_f consecutive frames, each of duration T_f. The transmit-pulse waveform $w(t)$ has typical duration T_w between 0.2–2 ns, which results in a transmission occupying an ultrawide bandwidth.

The physical multipath channel $g(t)$ can be expressed in terms of multipath delays and gains as

$$g(t) = \sum_{l_g=0}^{L_g-1} \alpha_g(l_g)\delta(t - \tau_g(l_g)) \tag{1}$$

where $\tau_g(l_g) > \tau_g(l_g - 1), \forall l_g \in [1, L_g - 1]$. As shown in Fig. 1, the overall channel $h(t)$ comprises the convolution of the pulse shaper $w(t)$ with the physical multipath channel $g(t)$, and is given by

$$h(t) := g(t) \star w(t) = \sum_{l_g=0}^{L_g-1} \alpha_g(l_g) w(t - \tau_g(l_g)) \tag{2}$$

where $\star$ stands for convolution. With $T_g := \tau_g(L_g - 1)$ denoting the maximum delay spread of the dense multipath channel, we avoid ISI by simply choosing $T_f \geq T_g + T_w$. We model the multipath fading channel as quasi-static, which is typical for an indoor environment. More precisely, we assume that $h(t)$ remains invariant over a symbol duration $N_f T_f$ seconds, but it is allowed to change from symbol to symbol.

The Rake receiver has L fingers, and employs $w(t)$ as the correlator template. MRC is performed at the receiver to yield the decision statistic. Based on the latter, an estimate of the transmitted symbol $\hat{s}$ is then formed by the detector.

When a single transmit antenna is deployed, the binary symbol s is transmitted with energy $\mathcal{E}$, using the symbol waveform

$$s(t) = s\sqrt{\frac{\mathcal{E}}{N_f}} \sum_{n_f=0}^{N_f-1} w(t - n_f T_f), \quad s = \pm 1 \tag{3}$$

where the pulse shaper $w(t)$ has unit energy, i.e., $\int_0^{T_f} w^2(t)\,dt = 1$. With a single receive antenna, and supposing that timing offsets have been compensated accurately, the received noisy waveform corresponding to s is given by $r(t) = s(t) \star g(t) + \eta(t)$, or, after using (3), $r(t) = s\sqrt{\mathcal{E}/N_f} \sum_{n_f=0}^{N_f-1} h(t - n_f T_f) + \eta(t)$, where $\eta(t)$ is the additive white Gaussian noise (AWGN) with zero mean, and variance σ^2.

The received waveform contains a large number of resolvable multipath components, due to the ultrashort duration of $w(t)$. In order to harvest the multipath diversity, a Rake receiver is employed at the receiver. Using the pulse shaper $w(t)$ as reference, a Rake receiver with L fingers yields the correlation of the received waveform $r(t)$ with L delayed versions of the reference waveform, namely, $\{w(t - \tau(l))\}_{l=0}^{L-1}$, where

$0 \leq \tau(0) < \tau(1) < \cdots < \tau(L-1) \leq T_g$. Notice that $\{\tau_g(l_g)\}_{l_g=0}^{L_g-1}$ in (2) denote the arrival times of the physical multipath components, which are merely determined by the physical environment. Therefore, no restrictions apply to the number and/or intervals of $\tau_g(l_g)$. On the other hand, the matched filter employing the template $w(t)$ can not resolve multipath components whose delays differ by less than one pulse duration T_w. Moreover, outputs of filters matched to $\{w(t-\tau_l)\}_{l=0}^{L-1}$ will be uncorrelated if $\{\alpha_g(l_g)\}_{l_g=0}^{L_g-1}$ are uncorrelated, and $\tau(l) - \tau(l-1) \geq 2T_w, \forall l \in [0, L-1]$. The latter can be guaranteed, since $\{\tau(l)\}_{l=0}^{L-1}$ are up to our choice. There are different ways to select the L fingers [2]. Since optimizing the Rake is beyond the scope of this paper, we will simply choose $\tau(l) = 2lT_w, \forall l \in [0, L-1]$, where $L \leq L_g$. During each frame duration T_f, the output of the lth finger of the Rake receiver is given by

$$x(l) = s\sqrt{\frac{\mathcal{E}}{N_f}}\alpha(l) + \zeta(l), \quad \forall l \in [0, L-1] \tag{4}$$

where $\zeta(l) := \int_0^{T_f} \eta(t) w(t-\tau(l))\, dt$, and $\alpha(l) := \int_0^{T_f} h(t) w(t-\tau(l))\, dt$; i.e.,

$$\alpha(l) := \sum_{l_g=0}^{L_g-1} \alpha_g(l_g) R_w(\tau(l) - \tau_g(l_g)) \tag{5}$$

with $R_w(\tau) := \int_0^{T_f} w(t) w(t-\tau)\, dt$ denoting the autocorrelation function of $w(t)$. It is evident that $\zeta(l)$ has zero mean and variance σ^2, since $w(t)$ has unit energy. Also recall that the finger delays satisfy $\tau(l) - \tau(l-1) \geq T_w, \forall l \in [1, L-1]$; hence, $\zeta(l)$ is also white.

To maximize the signal-to-noise ratio (SNR), MRC is used to collect the multipath diversity in two levels: the MRC of L fingers of the Rake receiver per frame; and the MRC of the N_f frames corresponding to the same symbol.

To apply MRC, the receiver requires knowledge of $\{\alpha(l)\}_{l=0}^{L-1}$. Recalling (5), we deduce that knowledge of $\{\alpha(l)\}_{l=0}^{L-1}$ requires knowledge of both the multipath delays $\{\tau_g(l_g)\}_{l_g=0}^{L_g-1}$ and gains $\{\alpha_g(l_g)\}_{l_g=0}^{L_g-1}$. In other words, the physical channel $g(t)$ needs to be acquired through, e.g., the use of pilot waveforms [24]. Assuming that the receiver has perfect knowledge of $\{\alpha(l)\}_{l=0}^{L-1}$, the MRC output per received frame is [cf. (4)]

$$\begin{aligned} y(n_f) &= \sum_{l=0}^{L-1} x(l)\alpha(l) = s\sqrt{\frac{\mathcal{E}}{N_f}} \sum_{l=0}^{L-1} \alpha^2(l) + \sum_{l=0}^{L-1} \alpha(l)\zeta(l) \\ &= s\sqrt{\frac{\mathcal{E}}{N_f}}\mathcal{E}_g + \xi(n_f), \quad \forall n_f \in [0, N_f - 1] \end{aligned} \tag{6}$$

where $\mathcal{E}_g := \sum_{l=0}^{L-1} \alpha^2(l)$, and $\xi(n_f) := \sum_{l=0}^{L-1} \alpha(l)\zeta(l)$. Notice that $\mathcal{E}_g$ represents the energy captured by the Rake receiver with L fingers. For fixed $L, \mathcal{E}_g$ is determined by the channel $g(t)$, since $w(t)$ was designed to have unit energy. Also notice that $\xi(n_f)$ is still a white Gaussian noise with zero mean, but its variance is now given by $\mathcal{E}_g\sigma^2$.

With the channel remaining invariant over a symbol duration N_fT_f, the MRC of N_f frames amounts to summing up $\{y(n_f)\}_{n_f=0}^{N_f-1}$ in (6). The resulting decision statistic corresponding to the symbol s is given by

$$z = s\sqrt{N_f\mathcal{E}}\mathcal{E}_g + \sum_{n_f=0}^{N_f-1} \xi(n_f). \tag{7}$$

The white Gaussian noise in (7) has zero mean, and variance $N_f\mathcal{E}_g\sigma^2$. When the maximum-likelihood (ML) detector is used, we have the BER

$$\mathrm{P}\left(e \,\middle|\, \{\alpha(l)\}_{l=0}^{L-1}\right) = Q(\sqrt{\rho\mathcal{E}_g})$$

where $\rho := \mathcal{E}/\sigma^2$ denotes the transmit SNR, and $Q(x) := (1/\sqrt{2\pi}) \int_x^\infty \exp(-t^2/2)\, dt$ is the Gaussian tail function. Conditioned on $\mathcal{E}_g$, the Chernoff bound yields ([12, Ch. 2])

$$\mathrm{P}\left(e \,\middle|\, \{\alpha(l)\}_{l=0}^{L-1}\right) \leq \exp(-\rho\mathcal{E}_g/2).$$

Using the definition of $\mathcal{E}_g$ in (6), we have

$$\begin{aligned} \mathrm{P}\left(e \,\middle|\, \{\alpha(l)\}_{l=0}^{L-1}\right) &\leq \exp\left(-\rho \sum_{l=0}^{L-1} \alpha^2(l)/2\right) \\ &= \prod_{l=0}^{L-1} \exp(-\rho\alpha^2(l)/2). \end{aligned} \tag{8}$$

In indoor environments with multiple reflections and refractions, the gain of each path can be modeled as a Rayleigh distributed random variable, while the phase is a uniformly distributed random variable [9], [13]. Since UWB systems employ real signals, we are only interested in the real part of each path gain, which has Gaussian distribution with zero mean. As combinations of Gaussian random variables, $\alpha(l)$'s are also Gaussian distributed. If the finger delays are chosen such that $\tau(l) - \tau(l-1) \geq 2T_w, \forall l \in [1, L-1]$, then we have $\mathrm{E}[\alpha(l_1)\alpha(l_2)] = 0, \forall l_1 \neq l_2$. In other words, $\alpha(l_1)$ and $\alpha(l_2)$ are uncorrelated $\forall l_1 \neq l_2 \in [0, L-1]$. Letting $\beta(l) := \mathrm{E}[\alpha^2(l)]$, and averaging the conditional BER over independent Gaussian distributions of $\alpha(l)$, we establish the following result.

Proposition 1: The average BER of a single-antenna UWB system employing a L-finger Rake receiver is upper bounded at high SNR ($\mathcal{E} \gg \sigma^2$), by

$$\mathrm{P}(e) \leq (\beta_L\rho)^{-\frac{L}{2}} \tag{9}$$

with diversity gain given by $L/2$, and coding gain given by $\beta_L := (\prod_{l=0}^{L-1} \beta(l))^{1/L}$.

Proof: See Appendix I. ∎

Equation (9) confirms that as the number of fingers L increases, the diversity order also increases. Interestingly, it can be verified that the BER upper bound in (9) becomes $(\rho\beta_L/2)^{-L}$ if $\alpha(l)$'s are independent complex Gaussian random variables with variance $\beta(l)/2$ per dimension (see, e.g., [17]). This difference comes from the fact that UWB transmissions are real. To achieve higher diversity gains, the number of Rake fingers L can be increased by choosing either additional (denser) finger

delays, or larger finger delays. With additional $\tau(l)$'s, the mutual independence among $\alpha(l)$'s is violated. With larger $\tau(l)$, the generally decreasing power profile of the multipath channel will decrease the coding gain β_L. In fact, the diversity order comes from the energy capture of the Rake receiver. The energy capture, however, does not increase linearly with the number of fingers L [21]. As a result, large L does not necessarily benefit performance, but certainly increases the implementation complexity at the receiver. Therefore, a larger number of fingers L is less desirable, while performance requirements are yearning for higher diversity order. To this end, the analog STC schemes that we pursue next are well motivated.

III. Analog STC

Let us now consider a UWB system with $N_t = 2$ transmit antennas, and $N_r = 1$ receive antenna.[1] We denote the impulse response of the multipath fading channel from the mth transmit antenna to the receive antenna with $g_m(t), m = 0, 1$. The channels $g_0(t)$ and $g_1(t)$ are assumed to be mutually independent, and quasi-static over one symbol duration $N_f T_f$. Correspondingly, the composite channel from the mth transmit antenna to the receive antenna is given by $h_m(t) := g_m(t) \star w(t)$. Denoting the maximum delay spread of $g_m(t)$ with T_{g_m}, we have the overall maximum delay spread $T_g := \max\{T_{g_0}, T_{g_1}\}$. As with single-antenna transmissions, we avoid ISI by choosing the frame duration $T_f \geq T_g + T_w$. Without loss of generality, we will take N_f to be even throughout our analysis. Similar to [1], we will later see that our STC designs rely on the same transmission power, and yield the same rate, as in single-antenna transmissions.

A. STC Scheme I

During each symbol duration $N_f T_f$, we transmit from the zeroth transmit antenna

$$s_0(t) = s\sqrt{\frac{\mathcal{E}}{2N_f}} \sum_{n_f=0}^{N_f-1} (-1)^{n_f} w(t - n_f T_f) \tag{10}$$

and from the first transmit antenna

$$s_1(t) = s\sqrt{\frac{\mathcal{E}}{2N_f}} \sum_{n_f=0}^{N_f-1} w(t - n_f T_f) \tag{11}$$

where the factor $\sqrt{2}$ ensures transmit energy identical to single-antenna transmissions. Notice that one symbol is transmitted over N_f frames, as with single-antenna transmissions. The received noisy waveform corresponding to symbol s is given by

$$\begin{aligned} r(t) &= s_0(t) \star g_0(t) + s_1(t) \star g_1(t) + \eta(t) \\ &= s\sqrt{\frac{\mathcal{E}}{2N_f}} \sum_{n_f=0}^{N_f-1} [(-1)^{n_f} h_0(t - n_f T_f) + h_1(t - n_f T_f)] \\ &\quad + \eta(t). \end{aligned}$$

[1]For design, properties, and challenges associated with UWB antennas, even with $(N_t, N_r) = (1, 1)$ configurations, the reader is referred to [5], [11], and [15]. Apart from the cost of deploying one or two extra UWB antennas, in the $(2, 1), (1, 2)$, or $(2, 2)$ configurations considered here, no extra challenges emerge relative to those already present in single antenna.

Denoting the received waveform during evenly and oddly indexed frames of each symbol as $r_e(t)$ and $r_o(t)$, respectively, we have $r(t) = \sum_{n_f=0}^{N_f'-1} [r_e(t - 2n_f T_f) + r_o(t - 2n_f T_f - T_f)]$, where $N_f' := N_f/2$, and

$$\begin{aligned} r_e(t) &= s\sqrt{\frac{\mathcal{E}}{2N_f}} [h_0(t) + h_1(t)] + \eta_e(t) \\ r_o(t) &= s\sqrt{\frac{\mathcal{E}}{2N_f}} [h_1(t) - h_0(t)] + \eta_o(t). \end{aligned}$$

Feeding them to the Rake receiver with L fingers, the output of the lth finger is given by

$$\begin{aligned} x_e(l) &= s\sqrt{\frac{\mathcal{E}}{2N_f}} [\alpha_0(l) + \alpha_1(l)] + \zeta_e(l) \quad \text{for even frames} \\ x_o(l) &= s\sqrt{\frac{\mathcal{E}}{2N_f}} [\alpha_1(l) - \alpha_0(l)] + \zeta_o(l) \quad \text{for odd frames} \end{aligned}$$

where $\alpha_m(l) := \int_0^{T_f} h_m(t) w(t - \tau(l))\, dt$ for $m = 0, 1$. The MRC output is

$$\begin{aligned} y_e(n_f) &= s\sqrt{\frac{\mathcal{E}}{2N_f}} \sum_{l=0}^{L-1} [\alpha_0(l) + \alpha_1(l)]^2 + \xi_e(n_f) \\ y_o(n_f) &= s\sqrt{\frac{\mathcal{E}}{2N_f}} \sum_{l=0}^{L-1} [\alpha_1(l) - \alpha_0(l)]^2 + \xi_o(n_f) \end{aligned}$$

for evenly and oddly indexed frames, respectively. Notice that $\xi_e(n_f) := \sum_{l=0}^{L-1} [\alpha_0(l) + \alpha_1(l)] \zeta_e(l)$ and $\xi_o(n_f) := \sum_{l=0}^{L-1} [\alpha_1(l) - \alpha_0(l)] \zeta_o(l)$ are white Gaussian noise variables with zero mean and variances $\sigma_{\xi_e}^2 = \sigma^2 \sum_{l=0}^{L-1} [\alpha_0(l) + \alpha_1(l)]^2$ and $\sigma_{\xi_o}^2 = \sigma^2 \sum_{l=0}^{L-1} [\alpha_1(l) - \alpha_0(l)]^2$, respectively, $\forall n_f \in [0, N_f' - 1]$. Summing up $y_e(n_f)$ and $y_o(n_f)$ over the N_f frames corresponding to the symbol s, we have $z = s\sqrt{N_f \mathcal{E}/2}(\mathcal{E}_{g_0} + \mathcal{E}_{g_1}) + \sum_{n_f=0}^{N_f'-1} (\xi_e(n_f) + \xi_o(n_f))$, where $\mathcal{E}_{g_m} := \sum_{l=0}^{L-1} \alpha_m^2(l)$, and the zero-mean noise has variance given by $N_f \sigma^2 (\mathcal{E}_{g_0} + \mathcal{E}_{g_1})$.

For given channels $g_0(t)$ and $g_1(t)$, the BER associated with the ML detector is given by

$$\mathrm{P}\left(e \,\middle|\, \{\alpha_0(l), \alpha_1(l)\}_{l=0}^{L-1}\right) = Q\left(\sqrt{\rho \frac{\mathcal{E}_{g_0} + \mathcal{E}_{g_1}}{2}}\right) \tag{12}$$

which is upper bounded by the Chernoff bound

$$\begin{aligned} \mathrm{P}\left(e \,\middle|\, \{\alpha_0(l), \alpha_1(l)\}_{l=0}^{L-1}\right) &\leq \exp(-\rho(\mathcal{E}_{g_0} + \mathcal{E}_{g_1})/4) \\ &= \exp(-\rho \mathcal{E}_{g_0}/4) \cdot \exp(-\rho \mathcal{E}_{g_1}/4). \end{aligned}$$

Averaging over $\{\alpha_0(l), \alpha_1(l)\}_{l=0}^{L-1}$, the following result is obtained.

Proposition 2: With STC Scheme I, channel coherence time $N_f T_f$, and L-finger Rake reception, the average BER of a UWB system deploying $(N_t, N_r) = (2, 1)$ antennas is upper bounded at high SNR by

$$\mathrm{P}(e) \leq \left(\frac{\beta_L}{2} \rho\right)^{-L} \tag{13}$$

which implies a diversity order L and a coding gain $\beta_L/2$.

Compared with (9), this ST-coded transmission scheme doubles the diversity order, at the expense of a 3-dB loss in coding gain and the cost of deploying one extra transmit antenna.

B. STC Scheme II

Instead of transmitting the same symbol simultaneously from the two transmit antennas, we can transmit two consecutive symbols s_a and s_b alternately from each of the two transmit antennas. More specifically, over two symbol durations $2N_fT_f$, we transmit

$$s_0(t)=\sqrt{\frac{\mathcal{E}}{2N_f}}\sum_{n_f=0}^{N_f-1}[s_a w(t-2n_fT_f)-s_b w(t-2n_fT_f-T_f)] \tag{14}$$

from the zeroth transmit antenna, and

$$s_1(t)=\sqrt{\frac{\mathcal{E}}{2N_f}}\sum_{n_f=0}^{N_f-1}[s_b w(t-2n_fT_f)+s_a w(t-2n_fT_f-T_f)] \tag{15}$$

from the first transmit antenna.

During the first symbol duration, the received noisy waveform is given by

$$\begin{aligned}r(t)=\sqrt{\frac{\mathcal{E}}{2N_f}}\sum_{n_f=0}^{N_f'-1}&[s_a h_0(t-2n_fT_f)\\&+s_b h_1(t-2n_fT_f)+s_a h_1(t-2n_fT_f-T_f)\\&-s_b h_0(t-2n_fT_f-T_f)]+\eta(t).\end{aligned}$$

As we allow channels to change from symbol to symbol, let $g_m'(t)$ denote the impulse response of the frequency-selective channels from the mth transmit antenna to the receive antenna during the second symbol duration of N_fT_f, and let $h_m'(t)$ denote its corresponding composite channel. Then, the received noisy waveform over the second symbol duration is given by

$$\begin{aligned}r'(t)=\sqrt{\frac{\mathcal{E}}{2N_f}}\sum_{n_f=0}^{N_f'-1}&[s_a h_0'(t-2n_fT_f)\\&+s_b h_1'(t-2n_fT_f)+s_a h_1'(t-2n_fT_f-T_f)\\&-s_b h_0'(t-2n_fT_f-T_f)]+\eta(t).\end{aligned}$$

Let us first look at $r(t)$. Denoting the received waveform during even and odd frames with $r_e(t)$ and $r_o(t)$, respectively, we have $r(t)=\sum_{n_f=0}^{N_f'-1}[r_e(t-2n_fT_f)+r_o(t-2n_fT_f-T_f)]$, where

$$\begin{aligned}r_e(t)&=\sqrt{\frac{\mathcal{E}}{2N_f}}[s_a h_0(t)+s_b h_1(t)]+\eta_e(t)\\r_o(t)&=\sqrt{\frac{\mathcal{E}}{2N_f}}[s_a h_1(t)-s_b h_0(t)]+\eta_o(t).\end{aligned}$$

Feeding them to the Rake receiver with L fingers, the output of the lth finger is given by

$$\begin{aligned}x_e(l)&=\sqrt{\frac{\mathcal{E}}{2N_f}}[s_a\alpha_0(l)+s_b\alpha_1(l)]+\zeta_e(l)\\x_o(l)&=\sqrt{\frac{\mathcal{E}}{2N_f}}[s_a\alpha_1(l)-s_b\alpha_0(l)]+\zeta_o(l)\end{aligned}$$

for evenly and oddly indexed frames. The resulting MRC outputs are, respectively

$$\begin{aligned}y_a(n_f)&=s_a\sqrt{\frac{\mathcal{E}}{2N_f}}(\mathcal{E}_{g_0}+\mathcal{E}_{g_1})+\xi_a(n_f)\\y_b(n_f)&=s_b\sqrt{\frac{\mathcal{E}}{2N_f}}(\mathcal{E}_{g_0}+\mathcal{E}_{g_1})+\xi_b(n_f).\end{aligned}$$

Notice that $\xi_a(n_f):=\sum_{l=0}^{L-1}[\alpha_0(l)\zeta_e(l)+\alpha_1(l)\zeta_o(l)]$ and $\xi_b(n_f):=\sum_{l=0}^{L-1}[\alpha_1(l)\zeta_e(l)-\alpha_0(l)\zeta_o(l)]$ are both white Gaussian with zero mean, and variance $\sigma_{\xi_a}^2=\sigma_{\xi_b}^2=\sigma^2(\mathcal{E}_{g_1}+\mathcal{E}_{g_2})$.

Summing up y_a and y_b over the first N_f frames, we have

$$\begin{aligned}z_a(n_f)&=s_a\sqrt{\frac{N_f\mathcal{E}}{8}}(\mathcal{E}_{g_0}+\mathcal{E}_{g_1})+\sum_{n_f=0}^{N_f'-1}\xi_a(n_f)\\z_b(n_f)&=s_b\sqrt{\frac{N_f\mathcal{E}}{8}}(\mathcal{E}_{g_0}+\mathcal{E}_{g_1})+\sum_{n_f=0}^{N_f'-1}\xi_b(n_f)\end{aligned}$$

where the two noise terms have identical variance $N_f\sigma^2(\mathcal{E}_{g_0}+\mathcal{E}_{g_1})/2$. Notice that the MRC also separates the outputs corresponding to the two symbols, and thereby decouples the detection of s_a and s_b.

After carrying out the same steps for the second received waveform $r'(t)$, we have outputs of the MRC-Rake receiver given by

$$\begin{aligned}z_a'&=s_a\sqrt{\frac{N_f\mathcal{E}}{8}}(\mathcal{E}_{g_0'}+\mathcal{E}_{g_1'})+\sum_{n_f=0}^{N_f'-1}\xi_a'(n_f)\\z_b'&=s_b\sqrt{\frac{N_f\mathcal{E}}{8}}(\mathcal{E}_{g_0'}+\mathcal{E}_{g_1'})+\sum_{n_f=0}^{N_f'-1}\xi_b'(n_f)\end{aligned}$$

where the variance of the two noise terms is $N_f\sigma^2(\mathcal{E}_{g_0'}+\mathcal{E}_{g_1'})/2$. Combining z_a and z_b with z_a' and z_b', respectively, we find the BER associated with the ML detector as

$$\begin{aligned}&\mathrm{P}\left(e\,\middle|\{\alpha_0(l),\alpha_1(l),\alpha_0'(l),\alpha_1'(l)\}_{l=0}^{L-1}\right)\\&\qquad=Q\left(\sqrt{\rho\frac{\mathcal{E}_{g_0}+\mathcal{E}_{g_1}+\mathcal{E}_{g_0'}+\mathcal{E}_{g_1'}}{4}}\right)\end{aligned}$$

which gives rise to the following result.

Proposition 3: With STC Scheme II, channel coherence time N_fT_f, and L-finger Rake reception, the average BER of a UWB

system deploying $(N_t, N_r) = (2, 1)$ antennas is upper bounded at high SNR by

$$\mathrm{P}(e) \leq \left(\frac{\beta_L}{4}\rho\right)^{-2L}$$

which implies a diversity order $2L$ and a coding gain $\beta_L/4$.

This ST-coded transmission scheme provides twice the diversity order of (13), without increasing either the number of Rake receiver fingers, or the channel estimation burden. The price paid relative to Scheme I is longer decoding delay. The transmission rates are common, namely, one symbol per N_f frames, as in the single-antenna case. A couple of remarks are now in order.

Remark 1: Different from Alamouti's scheme that encodes *across* digital symbols, our ST-coding scheme encodes analog waveforms *within* each symbol. To see the difference through an example, let us first define the symbol-level pulse shaper $w_s(t) := \sum_{n=0}^{N_f-1} w(t-nT_f)$. Encoding two consecutive digital symbols s_a and s_b with Alamouti's scheme forms the following ST matrix:

$$\begin{bmatrix} s_a & -s_b \\ s_b & s_a \end{bmatrix}.$$

We obtain at the pulse-shaper output $\forall t \in [0, 2N_fT_f)$

$$\begin{aligned} s_0(t) &= s_a\sqrt{\frac{\mathcal{E}}{2N_f}}w_s(t) - s_b\sqrt{\frac{\mathcal{E}}{2N_f}}w_s(t-N_fT_f) \\ s_1(t) &= s_b\sqrt{\frac{\mathcal{E}}{2N_f}}w_s(t) + s_a\sqrt{\frac{\mathcal{E}}{2N_f}}w_s(t-N_fT_f) \end{aligned} \quad (16)$$

from the two transmit antennas, over two symbol durations. Comparing (16) with (10) and (11), and (14) and (15), we deduce that our UWB-specific ST-coding Schemes I and II are different from the analog form of Alamouti's ST code. Interestingly, our STC Scheme II is the analog counterpart of Alamouti's ST code over pairs of frames [1].

Remark 2: *Propositions 2* and *3* show that if the channel coherence time is N_fT_f, then Scheme I has higher coding gain and lower diversity order than Scheme II. However, mimicking the proofs of *Propositions 2* and *3*, it can be shown that when the channel coherence time is at least $2N_fT_f$, Schemes I and II have identical diversity order and coding gain, which, in fact, coincide with those of the analog version of Alamouti's code in (16).

For the two PAM-based analog STC schemes, the MRC-Rake receiver employed requires estimation of the physical channels $\{g_m(t)\}_{m=0}^{1}$. Channel estimation using pilot waveforms reduces bandwidth efficiency, and increases the receiver complexity [24]. We will discuss later the possibility of noncoherent reception, which requires no channel state information.

IV. Generalizations

So far, we have developed two analog STC schemes for multi-antenna systems deploying $N_t = 2$ transmit and $N_r = 1$ receive antennas. By exploiting the space dimension, both schemes increase the diversity order without increasing the number of Rake fingers. This is due to the fact that not only the multipath diversity is collected with Rake reception, but also the spatial diversity is enabled with STC, and collected with MRC. Later on, we will verify the preceding analyses through numerical simulations. In this section, we are going to point out alternatives and generalizations of our STC schemes, and discuss issues pertaining to modulation, implementation, and multiple receive antennas.

A. Analog STC for PPM

With binary PPM, symbol -1 is represented by the pulse $w(t)$, while symbol $+1$ is represented by the delayed pulse $w(t-\Delta)$, where Δ is a delay up to the designer's choice. Accordingly, the frame duration has to be chosen to satisfy $T_f \geq T_g + T_w + \Delta$ to avoid ISI. The delay Δ (a.k.a. the modulation index) can be chosen to minimize the correlation $\int_0^{T_f} w(t)w(t-\Delta)\,dt$, and is given by $\Delta = 0.156$ ns [14]; Δ can also be designed to yield $\int_0^{T_f} w(t)w(t-\Delta)\,dt = 0$, so that $w(t)$ is orthogonal to $w(t-\Delta)$. Evidently, all $\Delta \geq T_w$ will result in orthogonal PPM. Among those orthogonal PPM designs, choosing $\Delta = T_g + T_w$ yields a transmission equivalent to a block-coded on–off keying (OOK) transmission, where symbol "-1" is represented by transmitting pulses during evenly indexed frames, and the opposite for symbol "$+1$" [3]. OOK ensures the orthogonality of the modulation, even after propagation through frequency-selective channels with maximum delay spread up to T_g. However, with the same pulse amplitude and symbol SNR, OOK results in approximately half the transmission rate of PAM or PPM with small Δ.

For PPM with arbitrary Δ, STC Scheme I can be applied without modification. At the Rake receiver, instead of $w(t-\tau(l))$, the correlators should use $w(t-\tau(l)-\Delta)-w(t-\tau(l))$ as their template. However, the STC Scheme II can only be applied to OOK signaling. This is because the multipath propagation destroys the orthogonality between the transmitted waveforms $w(t)$ and $w(t-\Delta)$ with any $\Delta < T_g+T_w$, and thereby prevents decoupling s_a from s_b.

B. Noncoherent Reception

In fact, when orthogonal PPM (with $\Delta = T_g + T_w$) is employed, noncoherent reception becomes possible. This is important because diversity collection and symbol detection can be performed without channel state information.

Applying STC Scheme I, the transmitted waveforms from the two transmit antennas are given by

$$\begin{aligned} s_0(t) &= \sqrt{\frac{\mathcal{E}}{2N_f}}\sum_{n_f=0}^{N_f-1}(-1)^{n_f}w(t-n_fT_f-\tilde{s}\Delta) \\ s_1(t) &= \sqrt{\frac{\mathcal{E}}{2N_f}}\sum_{n_f=0}^{N_f-1}w(t-n_fT_f-\tilde{s}\Delta) \end{aligned}$$

respectively, where $\tilde{s} := (s+1)/2$. Consequently, the received noisy waveform corresponding to symbol s is given by

$$\begin{aligned} r(t) = \sqrt{\frac{\mathcal{E}}{2N_f}}\sum_{n_f=0}^{N_f-1}[(-1)^{n_f}h_0(t-n_fT_f-\tilde{s}\Delta) \\ + h_1(t-n_fT_f-\tilde{s}\Delta)] + \eta(t). \end{aligned}$$

As in preceding sections, we can re-express the received waveform in terms of $r_e(t)$ and $r_o(t)$, which are now given by

$$r_e(t) = \sqrt{\frac{\mathcal{E}}{2N_f}}\,[h_0(t-\tilde{s}\Delta) + h_1(t-\tilde{s}\Delta)] + \eta_e(t)$$
$$r_o(t) = \sqrt{\frac{\mathcal{E}}{2N_f}}\,[h_1(t-\tilde{s}\Delta) - h_0(t-\tilde{s}\Delta)] + \eta_o(t) \quad (17)$$

respectively. Since $\Delta = T_g + T_w$, the maximum finger delay $\tau(L-1)$ is upper bounded by Δ. It then follows that $\int_0^{T_f} h_m(t-\Delta)w(t-\tau(l))\,dt = 0$, and $\int_0^{T_f} h_m(t)w(t-\tau(l)-\Delta)\,dt = 0, \forall l \in [0, L-1], m = 0, 1$. Consequently, in the absence of noise, the aggregate correlator output is given by

$$\boldsymbol{x}^{(s_0)}(l) = \begin{bmatrix} x_e(l) \\ x_o(l) \end{bmatrix} = \sqrt{\frac{N_f\mathcal{E}}{8}} \begin{bmatrix} \alpha_0(l)+\alpha_1(l) \\ \alpha_1(l)-\alpha_0(l) \end{bmatrix} \delta(s-s_0) + \begin{bmatrix} \eta_e(l) \\ \eta_o(l) \end{bmatrix}$$

which is associated with the template $w(t-\tau(l)-\tilde{s}_0\Delta)$ with $\tilde{s}_0 := (s_0+1)/2, s_0 = \pm 1$; $x_e(l)$ and $x_o(l)$ correspond to the even and odd indexed frames, respectively. Without knowledge of the channel, the energy detector turns out to be optimal [22]. Defining the decision statistic as

$$z(s_0) = \sum_{l=0}^{L-1} (\boldsymbol{x}^{(s_0)}(l))^T \boldsymbol{x}^{(s_0)}(l) = \sum_{l=0}^{L-1} \left\| \boldsymbol{x}^{(s_0)}(l) \right\|^2 \quad (18)$$

where $(\cdot)^T$ denotes transposition, the estimated symbol is given by $\hat{s} = \arg\max_{s_0} z(s_0)$.

In the absence of noise, (18) becomes $z(s_0) = (N_f\mathcal{E}/2)\sum_{l=0}^{L-1}[\alpha_0^2(l) + \alpha_1^2(l)]\delta(s-s_0)$, which implies that full space diversity of order two is achieved even with noncoherent reception. In other words, symbol detectability is guaranteed in the noise-free case, irrespective of channel realization.

When STC Scheme II is used, we have [cf. (17)]

$$r_e(t) = \sqrt{\frac{\mathcal{E}}{2N_f}}\,[h_0(t-\tilde{s}_a\Delta) + h_1(t-\tilde{s}_b\Delta)]$$
$$r_o(t) = \sqrt{\frac{\mathcal{E}}{2N_f}}\,[h_1(t-\tilde{s}_a\Delta) - h_0(t-\tilde{s}_b\Delta)]$$

for the first symbol duration consists of N_f frames, in the absence of noise. At the lth finger of the Rake receiver, we have combinations of the correlator outputs as follows:

$$y_1^{(s_1,s_2)}(n_f) = \int_0^{T_f} r_e(t)w(t-\tau(l)-\tilde{s}_1\Delta)\,dt - \int_0^{T_f} r_o(t)w(t-\tau(l)-\tilde{s}_2\Delta)\,dt$$
$$y_2^{(s_1,s_2)}(n_f) = \int_0^{T_f} r_e(t)w(t-\tau(l)-\tilde{s}_2\Delta)\,dt + \int_0^{T_f} r_o(t)w(t-\tau(l)-\tilde{s}_1\Delta)\,dt$$

where $\tilde{s}_m = \pm 1, m = 1, 2$. Collecting $y_m(n_f)$'s over the duration of the first N_fT_f seconds, we have in the absence of noise

$$\boldsymbol{y}^{(s_1,s_2)}(l) = \sum_{n_f=0}^{N_f'-1} \begin{bmatrix} y_1^{(s_1,s_2)}(n_f) \\ y_2^{(s_1,s_2)}(n_f) \end{bmatrix} = \sqrt{\frac{N_f\mathcal{E}}{8}}\alpha_0(l) \begin{bmatrix} \delta(s_a-s_1)+\delta(s_b-s_2) \\ \delta(s_a-s_2)-\delta(s_b-s_1) \end{bmatrix} + \sqrt{\frac{N_f\mathcal{E}}{8}}\alpha_1(l) \begin{bmatrix} \delta(s_b-s_1)-\delta(s_a-s_2) \\ \delta(s_b-s_2)+\delta(s_a-s_1) \end{bmatrix}.$$

Similarly, during the second symbol duration of N_fT_f seconds, we have $\boldsymbol{y}'^{(s_1,s_2)}(l)$, which bears the same form as $\boldsymbol{y}^{(s_1,s_2)}(l)$, but with $\alpha_m'(l)$ in place of $\alpha_m(l)$ due to possible variation of the channel. Consequently, pairs of symbols can be detected as $(\hat{s}_a, \hat{s}_b) = \arg\max_{(s_1,s_2)} z(s_1, s_2)$, where the decision statistic is given by

$$z(s_1,s_2) := \sum_{l=0}^{L-1} \left\| \boldsymbol{y}^{(s_1,s_2)}(l) \right\|^2 + \sum_{l=0}^{L-1} \left\| \boldsymbol{y}'^{(s_1,s_2)}(l) \right\|^2.$$

As with the previous case of STC Scheme I, it can be readily verified that symbol detectability is guaranteed in the absence of noise.

Remark 3: Among existing digital STC schemes, the unitary designs in [6] also allow for noncoherent reception. Our analog STC scheme, however, is different from [6] in the following aspects: 1) encoding in [6] takes place across symbols, whereas ours encode analog waveforms within symbols; and 2) noncoherent decoding in [6] does not guarantee symbol detectability even in the absence of noise, while our decoder exploits the orthogonal nonlinear PPM modulation to guarantee symbol detectability regardless of the channel realization, and thus enables full space diversity.

C. Antenna Switching

As we detailed in Section III-A, our analog STC Scheme I amounts to transmitting the same symbol simultaneously from both transmit antennas. Alternatively, this can be implemented with antenna switching. During each symbol duration, we transmit

$$s_0(t) = s\sqrt{\frac{\mathcal{E}}{N_f}} \sum_{n_f=0}^{N_f'-1} w(t-2n_fT_f)$$
$$s_1(t) = s\sqrt{\frac{\mathcal{E}}{N_f}} \sum_{n_f=0}^{N_f'-1} w(t-2n_fT_f-T_f)$$

from the two antennas, respectively. In other words, when one antenna transmits with full energy, the other one is shut off. Antenna switching is implemented digitally using a digital switch operating at the frame rate. Analog waveforms are forwarded to the two transmit antennas through two radio frequency (RF) arms, each being idle when the other is operating. The resulting conditional BER after the MRC-Rake reception and ML detection turns out to be the same as the one we found for Scheme I in (12). Therefore, this scheme provides the same coding gain and diversity order as Scheme I.

D. Interleaver Depth

STC Scheme II can be implemented by simply deploying an $N_f \times N_i$ block interleaver at the transmitter, with $N_i = 2$. The N_f repeated versions of s_a and s_b are fed to the interleaver columnwise and are read out rowwise. Actually, choosing the interleaver depth N_i to be any even factor of N_f, our STC Scheme II can be readily modified to achieve diversity order of LN_i with two transmit antennas, and MRC-Rake receiver with L fingers. Recall that the encoding and decoding of STC Scheme II are both performed in frame pairs. For any interleaver depth N_i, a symbol duration of N_f frames can be segmented into N_f/N_i groups each consisting of N_i frames. Grouping the N_i symbols into $N_i/2$ pairs, each pair can then be ST coded and transmitted over two consecutive frame durations. One round of the STC and transmission of the N_i symbols will take one group of N_i frames. Then the process is repeated for N_f times. Following the analysis in Section III-B, it can be readily verified that the average BER for any symbol is now upper bounded by

$$\mathrm{P}(e) \leq \left(\frac{\beta_L}{2N_i}\rho\right)^{-N_i L}$$

at high SNR. Achieving diversity order N_i times that provided by STC Scheme I [cf. (13)] with the identical L and same channel estimation complexity, comes at the price of decoding delay by N_i symbols, and loss in coding gain by a factor N_i.

E. STC with $N_r > 1$

With $N_t = 2$ transmit antennas, equipping the receiver with $N_r > 1$ antennas enables also receive diversity. Assuming that receive antennas are spaced sufficiently apart so that the channels are mutually uncorrelated, receive diversity can be readily exploited with MRC. It can then be shown that the upper bound of the averaged BER is given by

$$\mathrm{P}(e) \leq \left(\frac{\beta_L}{2}\rho\right)^{-N_r L}$$

for STC Scheme I, and

$$\mathrm{P}(e) \leq \left(\frac{\beta_L}{2N_i}\rho\right)^{-N_r N_i L}$$

for STC Scheme II, with an $N_f \times N_i$ block interleaver.

So far, we have focused on the case $N_t = 2$. In addition to allowing for analog ST transmitters, a unique feature of our STC schemes is that they do not suffer rate loss when $N_t > 2$ transmit antennas are deployed, simply because the PAM/PPM UWB transmissions are real by design [16].

V. Simulations

In this section, we present simulations and comparisons to validate our analyses and designs. In all cases, the random channels are generated according to [9] and [13], where rays arrive in several clusters within an observation window. The cluster arrival times are modeled as Poisson variables with cluster arrival rate Λ. Rays within each cluster also arrive according to a Poisson process with ray arrival rate λ. The amplitude of each arriving ray is a Rayleigh distributed random variable having exponentially decaying mean square value with parameters Γ and γ. Parameters of this channel model are chosen as $\Gamma = 33$ ns, $\gamma = 5$ ns, $1/\Lambda = 2$ ns, and $1/\lambda = 0.5$ ns. We select the pulse shaper $w(t)$ to be the second derivative of the Gaussian function $\sqrt{\tau^3/3}(2/\pi)^{1/4}\exp(-t^2/\tau^2)$. It can be verified that $w(t)$ has unit energy. The parameter τ is chosen to be 0.1225 ns to obtain a pulse width of 0.7 ns. The frame duration is chosen to be $T_f = 100$ ns [20], while the maximum delay spread is $T_g = 99$ ns.

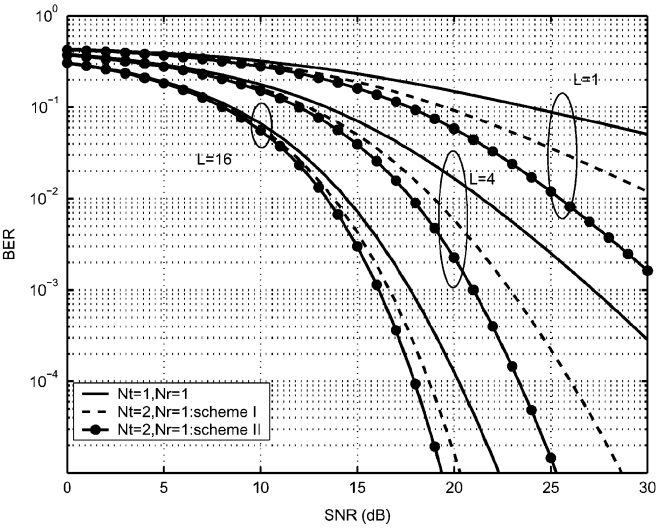

Fig. 2. BER performance comparison of single versus multiantenna UWB transmissions. L denotes the number of fingers of the Rake receiver.

1) Test Case 1: We first compare the BER performance of the single-antenna transmission, and our STC Schemes I and II with $N_t = 2$ and $N_r = 1$. With the number of fingers of the Rake receiver being $L = 1$, $L = 4$, and $L = 16$, the BER versus SNR curves are plotted in Fig. 2. For all L values, our STC schemes I and II provide, respectively, twice and four times the diversity order of the single-antenna transmission. Compared with a single-antenna transmission, our STC Scheme II with two transmit and one receive antennas is able to achieve the same diversity order with $1/4$ as many Rake fingers. Also notice that if $\beta_1 = \beta_4$, the coding gain difference between STC Scheme II with $L = 1$, and the single-antenna transmission with $L = 4$ should be 6 dB. However, from the figure, we observe that the coding gain loss is only 4 dB, which implies that β_4 is 2 dB less than β_1. Similarly, β_{16} is 3 dB less than β_4, and thus, 5 dB less than β_1. In other words, as L increases, β_L decreases, thus retaining part of the coding gain, as we predicted in Section II.

2) Test Case 2: With PAM modulation, we fix the number of fingers for the Rake receiver to $L = 1$. The number of transmit antennas is $N_t = 2$, and the number of receive antennas is $N_r = 1$. Our STC Scheme II is tested with various interleaver depths N_i. As we observe from Fig. 3, the diversity order increases with increasing N_i, as predicted in Section II, with increasing loss in coding gain, and longer decoding delay.

3) Test Case 3: When $N_r > 1$, excess diversity order can be obtained without losing coding gain. As depicted in Fig. 4, for both STC Schemes I and II, the deployment of an additional receive antenna doubles the diversity gain. Notice that Scheme

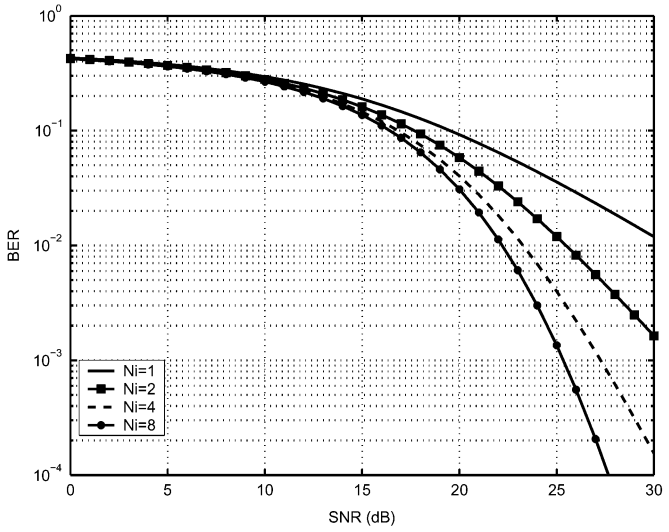

Fig. 3. Effects of the interleaver depth $N_i (N_t = 2, N_r = 1, L = 1)$.

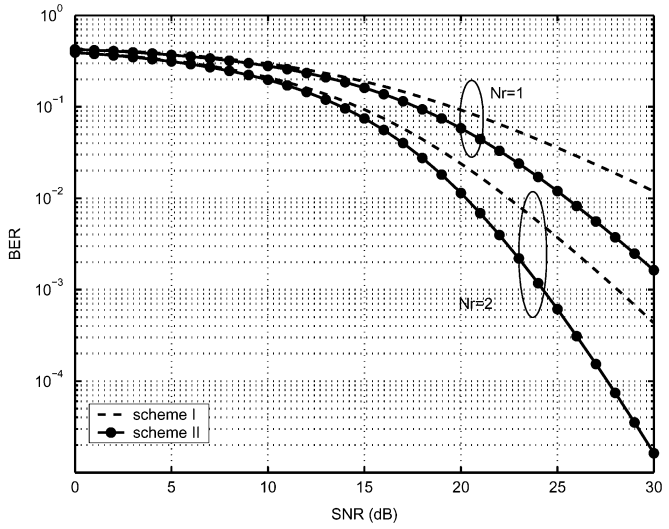

Fig. 4. Comparison of $N_r = 1$ and $N_r = 2$ cases for STC Schemes I and II $(N_t = 2, L = 1)$.

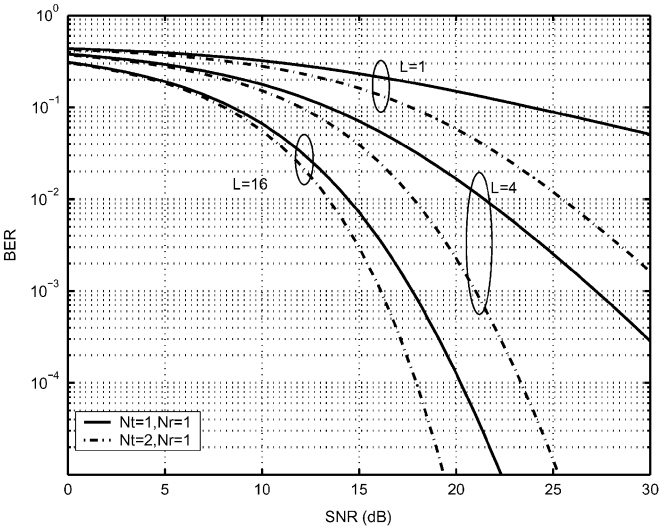

Fig. 5. BER performance in the absence of timing jitter. STC Scheme II is used when $N_t = 2$.

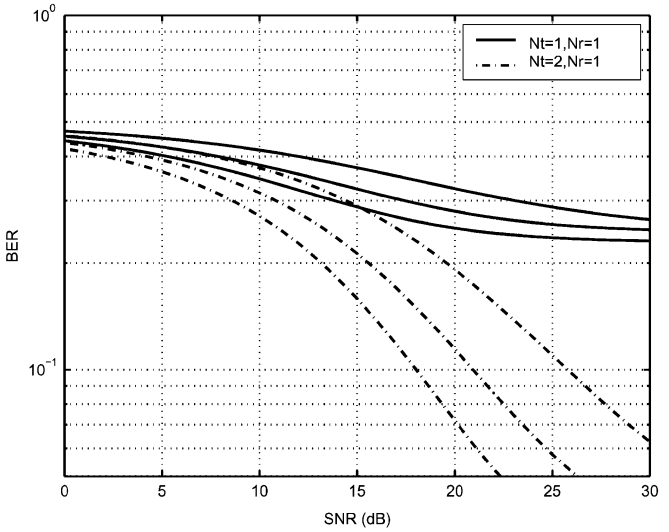

Fig. 6. BER performance in the presence of timing jitter. STC Scheme II is used when $N_t = 2$. The solid and dashed curves correspond to $L = 1$, $L = 4$, and $L = 16$ from top to bottom.

I with $N_r = 2$ provides the same diversity order, but 3 dB more coding gain than Scheme II with $N_r = 1$.

4) Test Case 4: In this case, we simulated the effects of timing jitter on BER performance for both single-antenna and multiantenna transmissions. Our STC Scheme II is used with $N_t = 2$ and $N_r = 1$. The timing jitter is modeled as an exponentially distributed random variable with mean 0.5 ns. Such a timing jitter could be catastrophic in AWGN channels, or flat-fading channels, because of the ultrashort pulse duration in UWB communications. In a dense multipath environment, however, some energy can still be captured, though considerable performance degradation occurs, as will be shown in our simulations. Fig. 5 depicts the BER versus SNR curves without timing jitter for $L = 1, 4$, and 16. It is evident from the figure that the diversity gain increases both with L and N_t. In the presence of timing jitter, great performance degradation is observed for both single- and multiple-antenna transmissions, as shown in Fig. 6. Nevertheless, multiple-antenna transmission outperforms single-antenna transmission for all L values. Furthermore, notice that larger L does not make much difference in the diversity order, while the benefit of multiple transmit antennas is still evident.

5) Test Case 5: With PPM modulation, the performance of single-antenna transmissions and our STC Scheme I with $N_r = 1$, and $N_r = 2$, is compared. As mentioned earlier, various modulation delays Δ can be employed in PPM. In this simulation example, we used two different Δ values: $\Delta = 0.156$ ns, which maximizes the correlation $\int_0^{T_f} w(t)[w(t) - w(t - \Delta)]\, dt$; and $\Delta = 1$ ns, which yields an orthogonal PPM. For both cases, the performance enhancement provided by higher diversity order can be observed from Fig. 7 for $L = 1$, and Fig. 8 for $L = 4$.

6) Test Case 6: Taking the modulation index $\Delta = T_g + T_w$, we also applied our STC Scheme II to OOK, a special case of PPM, with $N_r = 1$ and $N_r = 2$. Fig. 9 depicts the BER performance when coherent reception is applied. Fig. 10 depicts

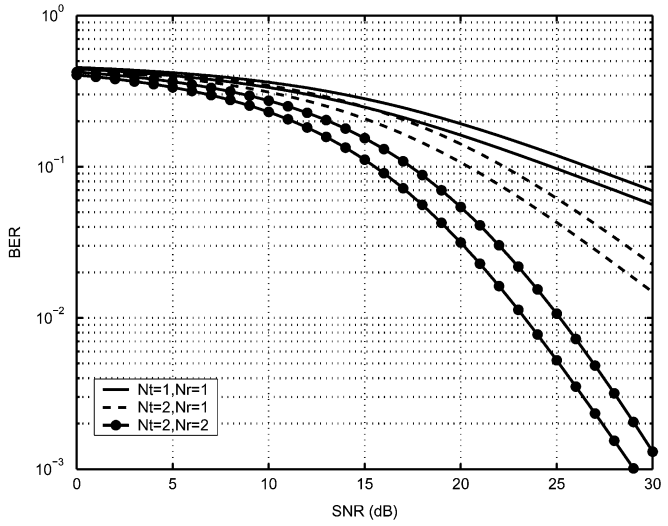

Fig. 7. STC Scheme I for PPM with $L = 1$. For each set of $\{N_t, N_r\}$, the upper curve is obtained with modulation delay $\Delta = 1$ ns, while the lower is obtained with $\Delta = 0.156$ ns.

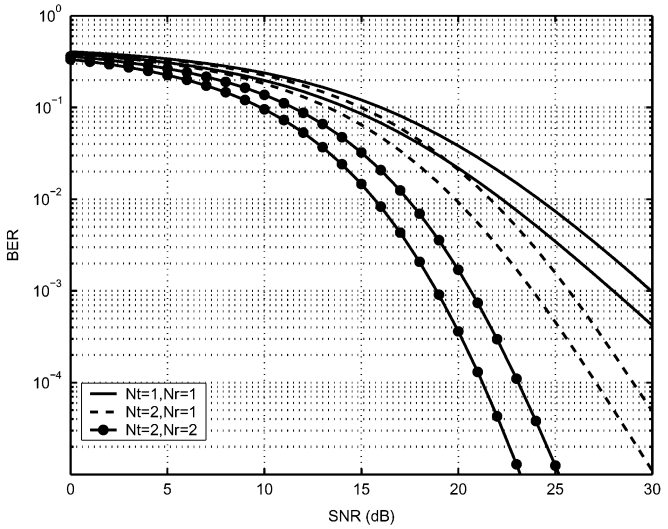

Fig. 8. STC Scheme I for PPM with $L = 4$. For each set of $\{N_t, N_r\}$, the upper curve is obtained with modulation delay $\Delta = 1$ ns, while the lower is obtained with $\Delta = 0.156$ ns.

the BER performance when noncoherent reception is employed. The combination of multipath and spatial diversity shows up clearly, although performance loss is observed in comparison with the coherent case, in return for the advantage of foregoing with channel estimation.

VI. Conclusion

In this paper, we developed analog STC schemes for multiantenna UWB transmissions. Conventional single-antenna UWB systems exploit multipath diversity provided by dense multipath indoor propagation channels with Rake receivers. We have shown that our STC schemes increase the diversity order without being necessary to increase the number of Rake fingers. Our designs can be applied to PPM with various modulation delays Δ, and enable flexible implementations with different diversity gains. Particularly, when OOK is used,

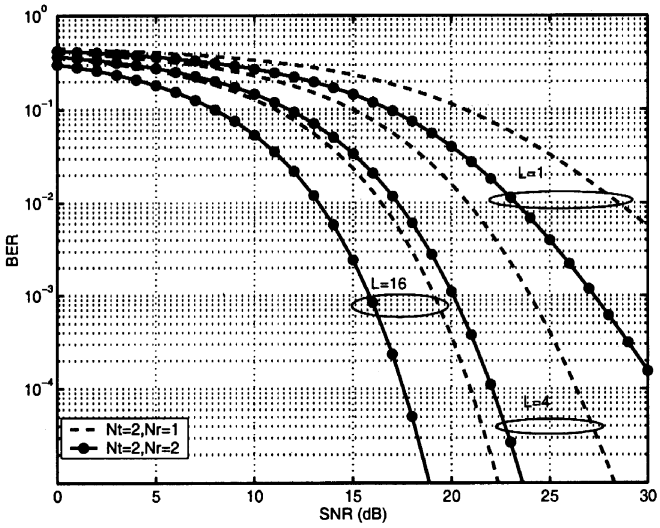

Fig. 9. STC for OOK modulation with coherent reception. Scheme II is used in both cases.

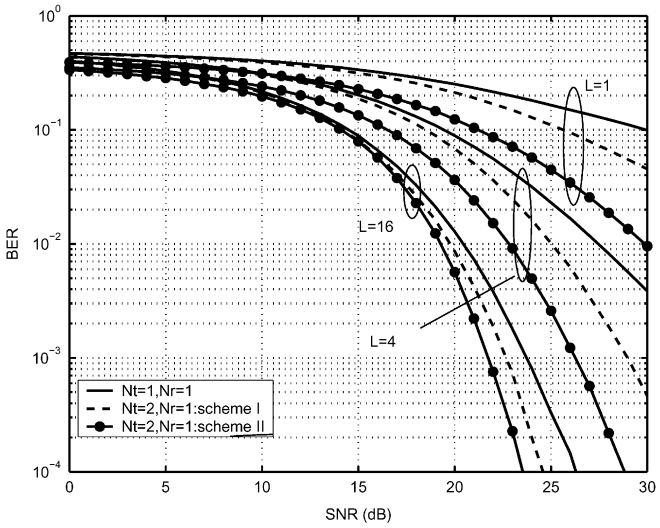

Fig. 10. STC for OOK modulation with noncoherent reception.

noncoherent reception can be deployed for collecting joint multipath and spatial diversity gains. Our STC schemes are tailored for UWB communications, and can be implemented in analog form with both PAM and PPM signaling. We have also revealed by simulations that our ST-coded transmissions exhibit robustness against timing jitter, which motivates us to exploit in the future multiple transmit and/or receive antennas for timing synchronization of UWB communication systems. From a UWB antenna design standpoint, coupling effects are also worth investigating.

Appendix I

Let us first define $\beta(l) := \mathrm{E}[\alpha^2(l)]$ as the expected energy per Rake finger. Then, averaging the conditional BER (8) over independent Gaussian distributions of $\alpha(l)$ yields the average BER bounded as follows:

$$\mathrm{P}(e) \leq \prod_{l=0}^{L-1} \mathrm{E}[\exp(-\rho\alpha^2(l)/2)] = \prod_{l=0}^{L-1} (1+\rho\beta(l))^{-\frac{1}{2}}.$$

At high SNR ($\mathcal{E} \gg \sigma^2$), the upper bound is given by

$$\mathrm{P}(e) \leq \left(\rho^L \prod_{l=0}^{L-1} \beta(l)\right)^{-\frac{1}{2}} = (\beta_L \rho)^{-\frac{L}{2}}$$

where $\beta_L := (\prod_{l=0}^{L-1} \beta(l))^{1/L}$. Casting the SNR ρ in decibels, (19) becomes

$$10 \log_{10} \mathrm{P}(e) \leq -\frac{L}{2}(10 \log_{10} \beta_L + \rho_{\mathrm{dB}})$$

which implies that the log-log plot of average BER versus SNR becomes a straight line at high SNR. The slope of the line is determined by $L/2$, and quantifies the diversity order; whereas a shift is introduced by β_L, which is known as coding gain.

REFERENCES

[1] S. M. Alamouti, "A simple transmit diversity technique for wireless communications," *IEEE J. Select. Areas Commun.*, vol. 16, pp. 1451–1458, Oct. 1998.

[2] D. Cassioli, M. Z. Win, F. Vatalaro, and A. F. Molisch, "Performance of low-complexity Rake reception in a realistic UWB channel," in *Proc. Int. Conf. Communications*, New York, NY, Apr. 28–May 2 2002, pp. 763–767.

[3] J. D. Choi and W. E. Stark, "Performance of ultra-wideband communications with suboptimal receivers in multipath channels," *IEEE J. Select. Areas Commun.*, vol. 20, pp. 1754–1766, Dec. 2002.

[4] J. R. Foerster, "The effects of multipath interference on the performance of UWB systems in an indoor wireless channel," in *Proc. Vehicular Technology Conf.*, Rhodes, Greece, Spring 2001, pp. 1176–1180.

[5] R. J. Fontana, E. A. Richley, A. J. Marzullo, L. C. Beard, R. W. T. Mulloy, and E. J. Knight, "An ultra-wideband radar for micro air vehicle applications," in *Proc. IEEE Conf. Ultra-Wideband Systems and Technologies*, Baltimore, MD, May 20–23, 2002, pp. 187–192.

[6] B. M. Hochwald and T. L. Marzetta, "Unitary space–time modulation for multiple-antenna communications in Rayleigh flat fading," *IEEE Trans. Inform. Theory*, vol. 46, pp. 543–564, Mar. 2000.

[7] S. S. Kolenchery, K. Townsend, and J. A. Freebersyser, "A novel impulse radio network for tactical wireless communications," in *Proc. IEEE MILCOM*, Bedford, MD, Oct. 18–21, 1998, pp. 59–65.

[8] C. Le Martret and G. B. Giannakis, "All-digital PAM impulse radio for multiuser communications through multipath," in *Proc. Global Telecommunications Conf.*, San Francisco, CA, Nov. 27–Dec. 1 2000, pp. 77–81.

[9] H. Lee, B. Han, Y. Shin, and S. Im, "Multipath characteristics of impulse radio channels," in *Proc. Vehicular Technology Conf.*, Tokyo, Japan, Spring 2000, pp. 2487–2491.

[10] W. M. Lovelace and J. K. Townsend, "The effects of timing jitter and tracking on the performance of impulse radio," *IEEE J. Select. Areas Commun.*, vol. 20, pp. 1646–1651, Dec. 2002.

[11] W. D. Prather, C. E. Baum, J. M. Lehr, J. P. O'Loughlin, S. Tyo, J. S. H. Schoenberg, R. J. Torres, T. C. Tran, D. W. Scholfield, J. Gaudet, and J. W. Burger, "Ultra-wideband source and antenna research," *IEEE Trans. Plasma Sci.*, vol. 28, pp. 1624–1630, Oct. 2000.

[12] J. Proakis, *Digital Communications*, 4th ed. New York: McGraw-Hill, 2001.

[13] A. A. M. Saleh and R. A. Valenzuela, "A statistical model for indoor multipath propagation," *IEEE J. Select. Areas Commun.*, vol. SAC-5, pp. 128–137, Feb. 1987.

[14] R. A. Scholtz, "Multiple access with time-hopping impulse modulation," in *Proc. IEEE MILCOM*, Boston, MA, Oct. 11–14, 1993, pp. 447–450.

[15] H. G. Schantz, "Radiation efficiency of UWB antennas," in *Proc. IEEE Conf. Ultra-Wideband Systems and Technologies*, Baltimore, MD, May 20–23, 2002, pp. 351–355.

[16] V. Tarokh, H. Jafarkhani, and A. R. Calderbank, "Space–time block codes from orthogonal designs," *IEEE Trans. Inform. Theory*, vol. 45, pp. 1456–1467, July 1999.

[17] V. Tarokh, N. Seshadri, and A. R. Calderbank, "Space–time codes for high-data-rate wireless communication: Performance criterion and code construction," *IEEE Trans. Inform. Theory*, vol. 44, pp. 744–765, Mar. 1998.

[18] J. D. Taylor, *Introduction to Ultra-Wideband Radar Systems*. Ann Arbor, MI: CRC Press, 1995.

[19] M. L. Welborn, "System considerations for ultra-wideband wireless networks," in *Proc. IEEE Radio and Wireless Conf.*, Boston, MA, Aug. 19–22, 2001, pp. 5–8.

[20] M. Z. Win and R. A. Scholtz, "Ultrawide bandwidth time-hopping spread-spectrum impulse radio for wireless multiple-access communications," *IEEE Trans. Commun.*, vol. 48, pp. 679–691, Apr. 2000.

[21] ——, "On the energy capture of ultrawide bandwidth signals in dense multipath environments," *IEEE Commun. Lett.*, vol. 2, pp. 245–247, Sept. 1998.

[22] L. Yang and G. B. Giannakis, "Space–time coding for impulse radio," in *Proc. IEEE Conf. Ultra Wideband Systems and Technologies*, Baltimore, MD, May 20–23, 2002, pp. 235–240.

[23] ——, "Multistage block-spreading for impulse radio multiple access through ISI channels," *IEEE J. Select. Areas Commun.*, vol. 20, pp. 1767–1777, Dec. 2002.

[24] L. Yang and G. B. Giannakis, "Optimal pilot-waveform-assisted modulation for ultra-wideband communications," *IEEE Trans. Wireless Commun.*, to be published.

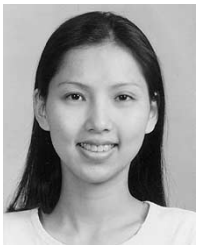

Liuqing Yang (S'02) received the B.S. degree from the Huazhong University of Science and Technology, Wuhan, China, in 1994, and the M.Sc. degree from the University of Minnesota, Minneapolis, in 2002, both in electrical engineering. She is currently working toward the Ph.D. degree in the Department of Electrical and Computer Engineering, University of Minnesota.

Her research interests include communications, signal processing, and networking. Currently, she has a particular interest in ultra-wideband (UWB) communications. Her research encompasses synchronization, channel estimation, equalization, multiple access, space–time coding, and multicarrier systems.

Georgios B. Giannakis (S'84–M'86–SM'91–F'97) received the Diploma in electrical engineering from the National Technical University of Athens, Greece, in 1981. He received the MSc. degree in electrical engineering in 1983, M.Sc. degree in mathematics in 1986, and the Ph.D. degree in electrical engineering in 1986, from the University of Southern California (USC), Los Angeles.

After lecturing for one year at USC, he joined the University of Virginia, Charlottesville, in 1987, where he became a Professor of Electrical Engineering in 1997. Since 1999, he has been with the University of Minnesota, Minneapolis, as a Professor in the Department of Electrical and Computer Engineering, and holds an ADC Chair in Wireless Telecommunications. His general interests span the areas of communications and signal processing, estimation and detection theory, time-series analysis, and system identification, subjects on which he has published more than 180 journal papers, 340 conference papers, and two edited books. Current research focuses on transmitter and receiver diversity techniques for single- and multiuser fading communication channels, comples-field and space–time coding, multicarrier, ultra-wideband wireless communication systems, cross-layer designs, and distributed sensor networks.

Dr. Giannakis is the corecipient of five Best Paper Awards from the IEEE Signal Processing (SP) Society (1992, 1998, 2000, 2001, and 2003). He also received the Society's Technical Achievement Award in 2000. He co-organized three IEEE-SP Workshops, and guest co-edited four special issues. He has served as Editor in Chief for the IEEE SIGNAL PROCESSING L ETTERS, as Associate Editor for the IEEE TRANSACTIONS ON SIGNAL PROCESSING and the IEEE SIGNAL PROCESSING LETTERS, as secretary of the SP Conference Board, as member of the SP Publications Board, as member and vice-chair of the Statistical Signal and Array Processing Technical Committee, and as chair of the SP for Communications Technical Committee. He is a member of the Editorial Board for the PROCEEDINGS OF THE IEEE, and the steering committee of the IEEE TRANSACTIONS ON WIRELESS COMMUNICATIONS. He is a member of the IEEE Fellows Election Committee, and the IEEE-SP Society's Board of Governors.